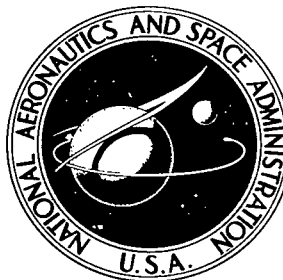


NASA TECHNICAL NOTE



NASA TN D-5895

C.1

NASA TN D-5895

LOAN COPY: RETURN  
AFWL (WLOL)  
KIRTLAND AFB, N



# EXPERIMENTAL INVESTIGATION OF CLOSE-RANGE ROCKET-EXHAUST IMPINGEMENT ON SURFACES IN A VACUUM

*by Leonard V. Clark*  
*Langley Research Center*  
*Hampton, Va. 23365*



0132637

1. Report No. NASA TN D-5895	2. Government Accession No.	3. Recipient's Catalog No.	
4. Title and Subtitle EXPERIMENTAL INVESTIGATION OF CLOSE-RANGE ROCKET-EXHAUST IMPINGEMENT ON SURFACES IN A VACUUM	5. Report Date July 1970		6. Performing Organization Code
	7. Author(s) Leonard V. Clark		8. Performing Organization Report No. L-6089
9. Performing Organization Name and Address NASA Langley Research Center Hampton, Va. 23365	10. Work Unit No. 124-08-29-01		11. Contract or Grant No.
	12. Sponsoring Agency Name and Address National Aeronautics and Space Administration Washington, D.C. 20546		13. Type of Report and Period Covered Technical Note
	15. Supplementary Notes		14. Sponsoring Agency Code
16. Abstract  An experimental ground-based program was conducted to investigate the effects of rocket-exhaust impingement on close-range surfaces. Although the configuration used in this investigation simulated the Apollo lunar module during lunar landing, the results are considered to be generally applicable to similar programs. A 1/10.5-scale model of the lunar module retrorocket with its base structure was fired at flat, dished, and particulate surfaces under near-vacuum conditions. Target-surface impingement pressures and heating rates, descent-stage base pressures, and nozzle static pressures were measured with the test rocket at various attitudes to the surface, altitudes above the surface, and operating thrust levels.			
17. Key Words (Suggested by Author(s)) Rocket-exhaust impingement Extraterrestrial landing Touchdown dynamics		18. Distribution Statement Unclassified - Unlimited	
19. Security Classif. (of this report) Unclassified	20. Security Classif. (of this page) Unclassified	21. No. of Pages 29	22. Price* \$3.00

**EXPERIMENTAL INVESTIGATION  
OF CLOSE-RANGE ROCKET-EXHAUST IMPINGEMENT  
ON SURFACES IN A VACUUM**

By Leonard V. Clark  
Langley Research Center

**SUMMARY**

An experimental ground-based program was conducted to investigate the effects of rocket-exhaust impingement on close-range surfaces. Although the configuration used in this investigation simulated the Apollo lunar module during lunar landing, the results are considered to be generally applicable to similar programs. A 1/10.5-scale model of the lunar module retrorocket with its base structure was fired at flat, dished, and particulate surfaces under near-vacuum conditions. Target-surface impingement pressures and heating rates, descent-stage base pressures, and nozzle static pressures were measured with the test rocket at various attitudes to the surface, altitudes above the surface, and operating thrust levels.

The results of the study indicate that surface impingement pressures were inversely proportional to rocket altitude but approached limiting maximum values at an altitude of approximately 2 rocket-exit diameters. For impingement normal to the surface, the maximum surface pressure equaled the value of shock-recovery pressure, but this pressure was considerably exceeded during off-normal tests. Pressures on the base of the model spacecraft caused by surface-reflected exhaust gases were one to two orders of magnitude less than target-surface pressures and were measurable only at rocket altitudes less than approximately 2 rocket-exit diameters, even during particulate target tests where eroded craters tended to reflect the rocket-exhaust gases toward the model spacecraft. In addition, the onset of nozzle choking as a result of surface proximity occurred at approximately the altitude at which the cylindrical escape area, formed between the rocket exit and the target surface, became less than the rocket-exit area (a rocket altitude of 0.25 rocket-exit diameter).

**INTRODUCTION**

Spacecraft which must soft-land on extraterrestrial surfaces having little or no atmosphere, such as the moon, require retrorockets to brake their approach velocities.

During touchdown, exhaust gases from these rockets impose pressure and temperature loads on the target surface which not only can alter the surface (e.g., erosion) but also can reflect onto the vehicle and may cause structural and/or landing stability problems. Previous studies of rocket-exhaust impingement (refs. 1 to 7) were concerned principally with determining the effects of direct rocket-exhaust impingement. Only references 1 and 2 also considered the effects of target-surface-reflected exhaust gases on nearby surfaces, like those on a spacecraft during rocket-braked landing. However, the studies of references 1 and 2 were exploratory and used only flat target surfaces and experimental configurations which were not representative of scaled spacecraft landers.

As part of an experimental study performed at the Langley Research Center, in support of the Apollo program, information was obtained for retrorockets operating near touchdown. A model of the lunar module (LM) retrorocket, surrounded by a similarly scaled LM base structure without landing gear, was fired onto solid and particulate surfaces in a large vacuum chamber at various attitudes to the surface, altitudes above the surface, and operating thrust levels. Measurements obtained during impingement onto flat and dished solid surfaces included static pressures and heating rates on the impinged surfaces, and static pressures on the LM model base and on the inside wall of the rocket nozzle. Pressure measurements on the LM model base were also obtained for a few tests with the rocket exhaust impinging on noncohesive particulate surfaces to determine the effects of cratering. Results of this study are presented herein.

## SYMBOLS

d	diameter
h	rocket altitude above target surface as measured from nozzle exit along rocket axis
p	pressure
r	radial distance measured along target surface from rocket axis
y	depth of soil erosion as measured from initial surface
$\beta$	surface inclination from horizontal; rocket-axis inclination from vertical
$\phi$	coordinate locating pressure gages on flat target surface

**Subscripts:**

b	LM model base
c	rocket combustion chamber
e	rocket nozzle exit
max	maximum
n	nozzle
r	shock-recovery conditions
s	surface
stag	rocket-axis impingement point (stagnation)
25	location of particular pressure orifice on flat target surface

**SIMULATION CONSIDERATIONS**

Laboratory studies of the problems associated with rocket-exhaust impingement on extraterrestrial surfaces during landing require reasonable simulation of the exhaust flow field and of the physical characteristics and behavior of the surface being impinged. Because exact duplication cannot be achieved in the laboratory, experiments must be carefully planned to produce meaningful results. Simulation and scaling for studies of this type are discussed in detail in references 5 and 8. Some considerations pertinent to the present study are discussed in this section.

The flow field of a free jet depends on the exhaust Mach number, the lip angle of the nozzle, and the ratio of combustion-chamber pressure to external pressure. When the jet impinges a surface, the flow is redirected and modified by shock and expansion waves which depend on the surface contour. All of these factors affect the energy distribution of the flow field and thus affect the pressure distributions both on the surface impinged directly by the jet and on the base of the descending vehicle.

The vehicle base pressure results in large part from the surface-reflected exhaust gases rather than from the exhaust flow field of the free jet. Therefore, changes in surface contour by jet erosion of surface particles could significantly influence base pressure,

particularly if erosion causes a dished-shape crater which would tend to reverse the flow. Erosion depends not only on the flow field over the surface but also on the properties of the particles; for example, the aerodynamic drag of the particles, interparticle cohesion, particle interlocking, and particle frictional restraint resulting from gravity. The studies of reference 5 showed, for example, that noncohesive soils erode at a much faster rate and form more symmetrical bowl-shape craters than do cohesive soils. Surface temperature resulting from exhaust impingement depends not only on all the flow-field properties previously mentioned but also on rocket combustion-chamber pressure (ref. 2). Thus, a variety of factors must be considered in experiments where surface pressure and temperature distributions are to be measured.

The experiments of the present study approximately simulated the terminal descent of the LM to the lunar surface. The model rocket engine used the same propellant as the LM and had approximately the same scaled nozzle contour but was somewhat fore-shortened. The test rocket had a slightly lower Mach number and nozzle-exit lip angle.

The large vacuum chamber where the experiments were conducted was evacuated to a pressure of approximately  $4 \times 10^{-4}$  torr ( $1 \text{ torr} = 133.22 \text{ N/m}^2$ ) prior to each of the tests. After 0.1 second of rocket engine firing, the chamber pressure had reached  $1.3 \times 10^{-3}$  torr; after 0.5 second,  $6 \times 10^{-2}$  torr. Because the chamber pressure was substantially greater than lunar ambient pressure ( $10^{-14}$  torr), the ratio of combustion-chamber pressure to external pressure was less than ideal. Fortunately, a lower ratio still allows near matching of the energy distribution of that portion of the jet flow field considered to influence pressure and temperature distributions. A pressure ratio of  $10^5$  is probably acceptable. For the present study, the ratio ranged between  $0.6 \times 10^5$  and  $130 \times 10^5$ . The exhaust-plume expansion angle, calculated to be  $97^\circ$  for the LM, ranged from  $62^\circ$  to  $67^\circ$  for the present solid-surface impingement tests and from  $47^\circ$  to  $67^\circ$  for the particulate-surface impingement tests. The experimental pressure data are likely to be somewhat higher than full-scale data because of the difference in plume angle. Any difference, however, is probably within the accuracy of the pressure gages used during the present study.

The effects of landing surface contour on LM model base pressures were evaluated with both a solid dished surface of arbitrary radius and an erodible particulate surface. Although subsequent observations on the moon indicate little cratering from the retrorocket due apparently to the cohesive nature of the particles, a worst-case approach was followed in the present study and noncohesive readily erodible particles were used. Only qualitative information could be expected from the erosion tests since the simulation did not encompass either the lunar-gravity condition or the LM descent velocity-time profile.

Heating produced by direct rocket-exhaust impingement increases with increasing combustion-chamber pressure and with decreasing altitude. In the present study, heating data were obtained at various fixed altitudes but at only one value of combustion-chamber pressure, which was considerably higher than the value for the LM retrorocket during landing. Although the test combustion-chamber temperature is probably about the same as that for the LM retrorocket ( $\approx 3100^{\circ}$  K), the heating rates are likely to be somewhat higher than full-scale values because of the higher combustion pressure and the relatively underexpanded rocket exhaust plume.

## APPARATUS

### General Setup

The experimental investigation was conducted at the Langley Research Center in the 41-foot-diameter (12.5-meter) vacuum sphere, which has a vacuum capability of  $2 \times 10^{-4}$  torr. The test apparatus is shown installed in this facility in the photograph of figure 1. The test rocket was positioned so that its exhaust gases impinged upon an instrumented target surface, which could be positioned, by remote control, between rocket firings.

### Test Rocket

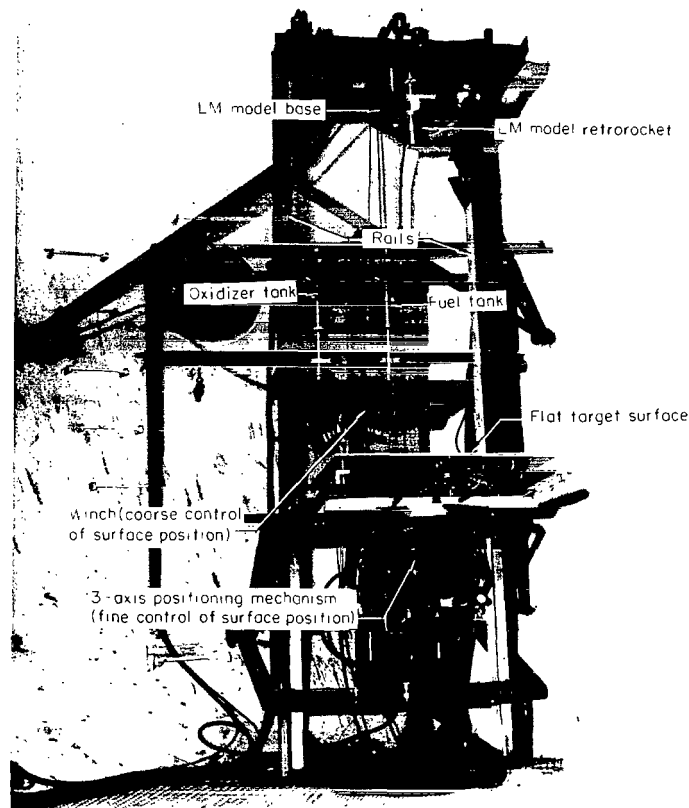
The LM retrorocket was simulated by a liquid-propellant rocket having a nominal thrust rating of 445 newtons. The test rocket is a duplicate of one of the sixteen rockets used on the LM spacecraft for attitude control. It has about the same nozzle contour as the LM retrorocket and, based on the rocket nozzle-exit diameter, can be considered a 1/10.5-scale model. The test rocket nozzle has an exit diameter of 13.9 cm, with an expansion ratio of 39.6 and an exit lip angle of  $8.3^{\circ}$ . The LM retrorocket nozzle has an expansion ratio of 47 and an exit lip angle of  $9.6^{\circ}$ . The test rocket and the LM retrorocket burn the same hypergolic propellants, nitrogen tetroxide and a mixture of 50 percent hydrazine and 50 percent unsymmetrical dimethylhydrazine. For the present tests, the ratio of oxidizer to fuel mixture was 2/1.

The test rocket was not designed to operate at combustion pressures below about  $450 \text{ kN/m}^2$  and therefore could not completely simulate the LM retrorocket condition at touchdown ( $170 \text{ kN/m}^2$ ) prior to thrust termination. Previous investigations have shown, however, that impingement pressures are directly proportional to the rocket combustion pressure. (See ref. 4.) To verify this fact and to demonstrate data repeatability, the majority of the present tests were conducted at three different rocket combustion pressures: 650, 550, and  $450 \text{ kN/m}^2$ . At a combustion pressure of  $650 \text{ kN/m}^2$ , the test rocket produces approximately 445 newtons of thrust with an estimated exhaust-exit Mach number of 4.53 for a gas specific-heat ratio of 1.25.

One phase of the study was devoted to determining the rocket altitude at which the exhaust flow separated in the nozzle as a result of the proximity of the target impingement surface. Measurement of exhaust static pressures at several locations within the rocket nozzle was undertaken in order to detect such choked-flow conditions.

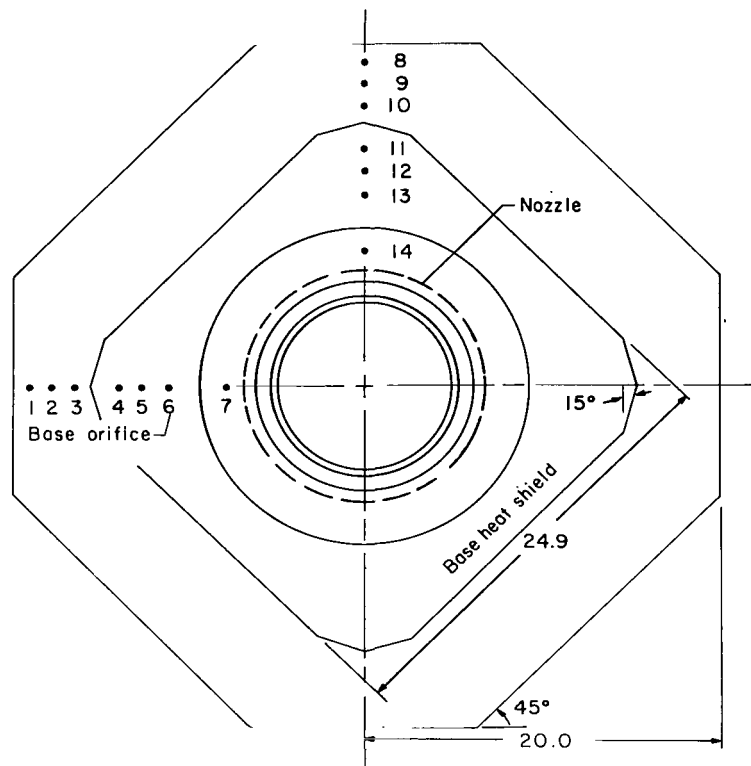
### LM Model Base

To simulate physically the LM spacecraft during landing, a 1/10.5-scale model of the bottom of the LM descent stage, without landing gear, was mounted around the test rocket as shown in the photograph of figure 1. This base, depicted schematically in figure 2, was equipped with a total of 14 orifices for measuring static pressure. These orifices were distributed along two perpendicular axes of symmetry, and each orifice was linked to a differential pressure gage (referenced to ambient pressure) with a short length of plastic tubing. The position of the LM model base with respect to the test rocket was similar to that of the prototype spacecraft.

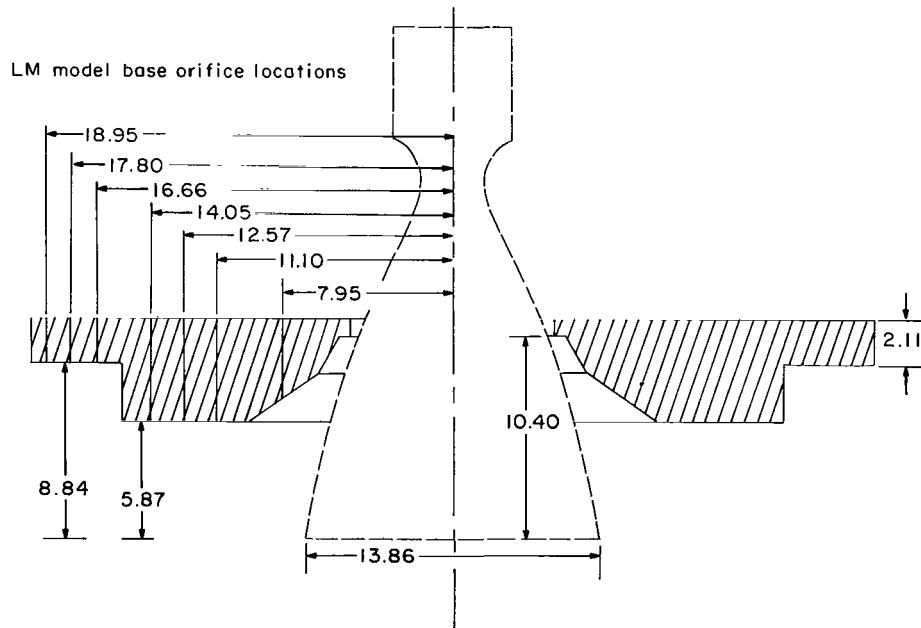


L-66-6682

Figure 1.- Photograph of test setup in 41-foot-diameter (12.5-meter) vacuum sphere at Langley Research Center.



(a) Bottom view.

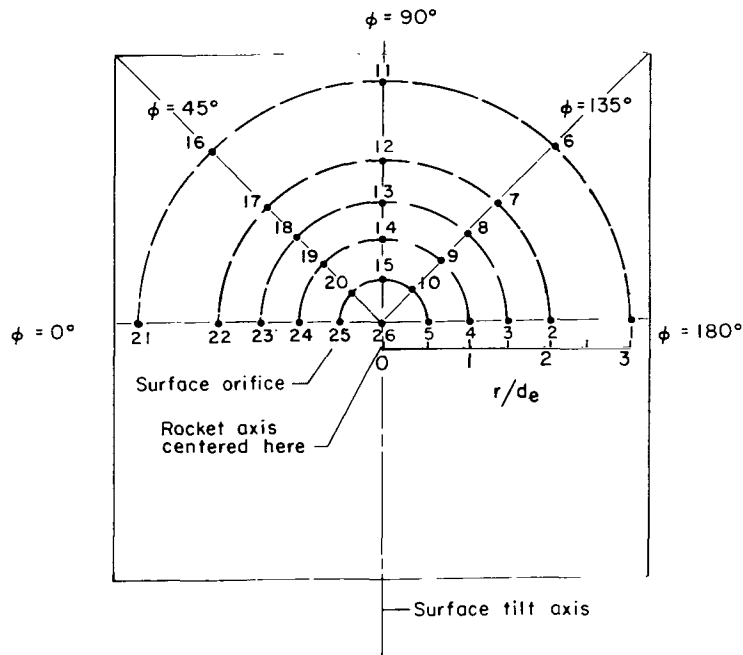


(b) Cross-sectional view showing position of test rocket.

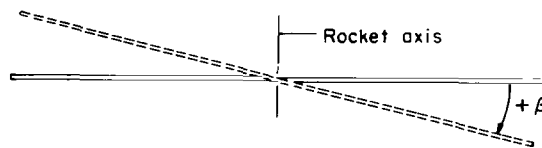
Figure 2.- Schematic of IM model base showing pressure-orifice locations. All dimensions are given in cm unless otherwise indicated.

## Target Surfaces

Impingement targets for the present tests consisted of flat, dished, and particulate surfaces. The principal target surface was a 91-cm square flat plate instrumented as shown in figure 3 to measure impingement static pressures. Another flat surface having the same dimensions was instrumented with calorimeters to measure impingement heating rates at several locations. The dished impingement surface, shown schematically in figure 4, was considered to be somewhat representative of a crater or an eroded depression



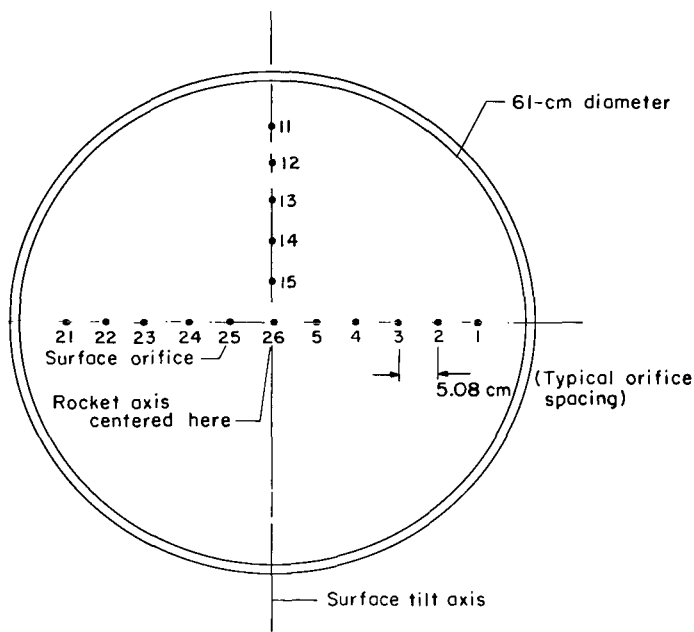
(a) Top view.



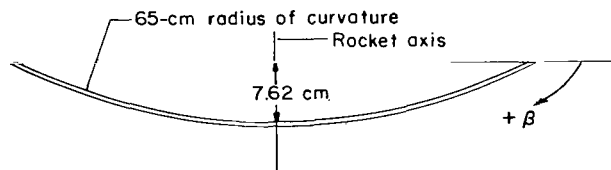
(b) Side view.

Figure 3.- Schematic of flat target surface, 91-cm square, showing pressure-orifice locations.

produced by the interaction of the rocket exhaust with the lunar surface. The dished surface was instrumented to measure impingement static pressures at the orifice locations detailed in figure 4. Finally, a few tests were conducted on a particulate surface measuring 91 cm in diameter and 15 cm in depth. In order for the rocket exhaust to produce a reasonable-size crater, noncohesive test soils were chosen. (See ref. 5.) The distribution of particle size of two simulated lunar soils is shown in figure 5. The soil mixture is a combination by weight of 25 percent lava cinders, 50 percent crushed sandstone, and 25 percent pumice.



(a) Top view.



(b) Side view.

Figure 4.- Schematic of dished target surface showing pressure-orifice locations.

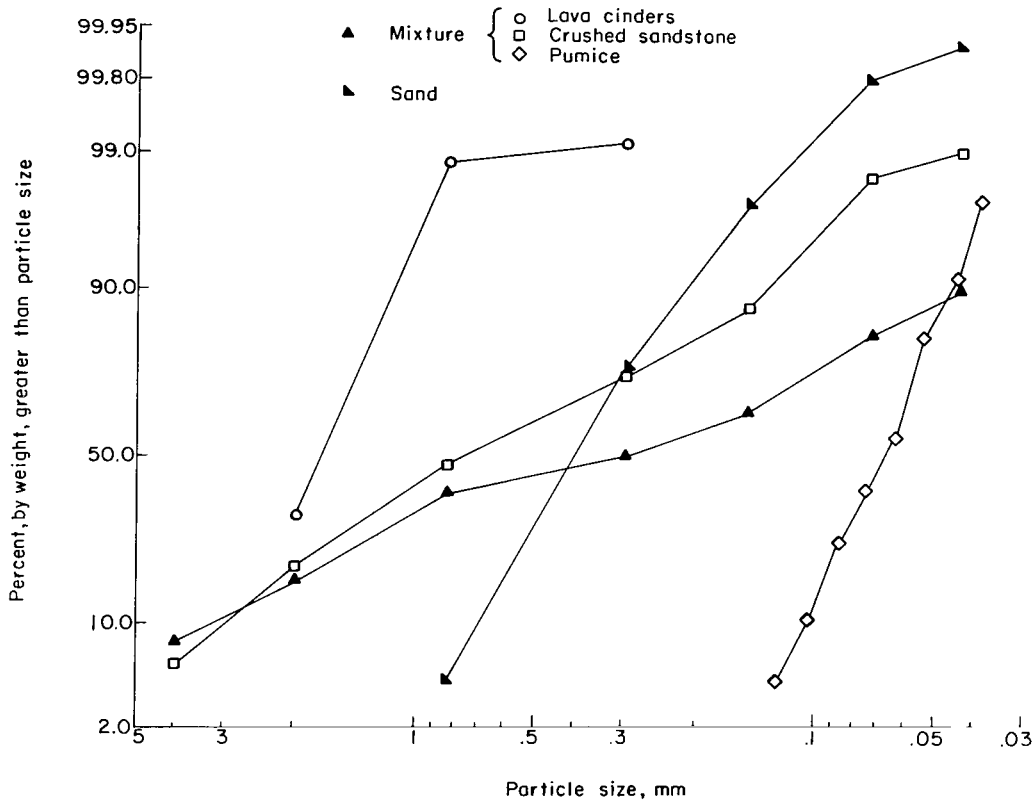


Figure 5.- Particle-size distribution analysis of simulated lunar soils.

### Instrumentation

All impingement and nozzle pressures were measured with inductance-type differential gages (referenced to the vacuum chamber from a common manifold) having capacities of 3.4 to 103 kN/m<sup>2</sup>. The rocket combustion-chamber pressure was measured with a 689-kN/m<sup>2</sup>-capacity strain gage, and the vacuum-chamber ambient pressure was measured with a cold-cathode gage. Heating rates were determined with 1.07-cm-diameter, 0.076-cm-thick, copper-disk calorimeters that were insulated from the impingement surface. Details of the construction and installation of the calorimeters are given in figure 6.

Coarse control over the distance between the surface and the test rocket was accomplished by moving the target surface toward the rocket along vertical rails with the aid of a motor-driven winch. (See fig. 1.) The location of the surface was determined by a scale mounted alongside the rails. The winch could be remotely actuated to stop the surface within 0.2 cm of a desired location. In addition, the test surface was mounted to a three-axis motor-driven positioning mechanism which permitted remote movement of

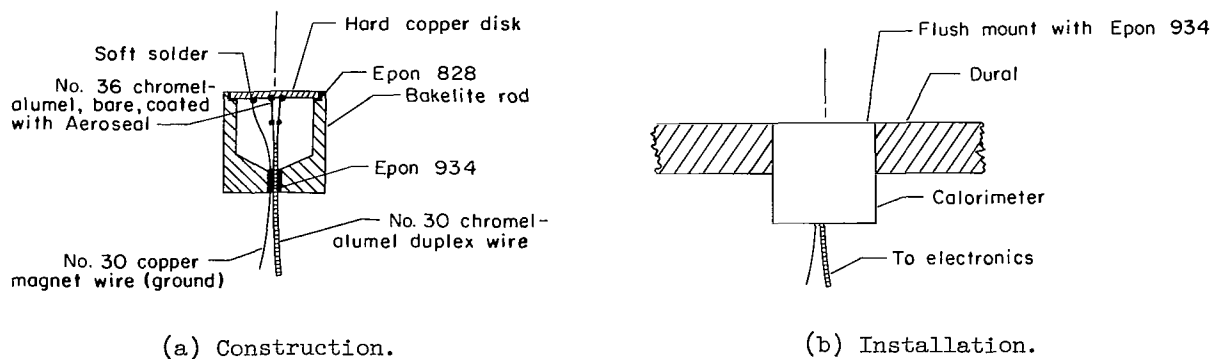


Figure 6.- Schematic of typical calorimeter gage.

the surface in the horizontal, vertical, and rotational directions. The positioning mechanism was used primarily to control the attitude of the test surface with respect to the rocket nozzle. The movement of the surface by this mechanism was monitored by linear-variable differential transducers which had outputs displayed on digital voltmeters calibrated to indicate movement to the nearest 0.02 cm vertically, 0.01 cm horizontally, and  $0.06^\circ$  rotationally. Close-range tests ( $h/d_e \leq 0.5$ ) employed only the positioning mechanism for moving the target surface. A mechanical stop on the rails was employed to provide positive indication of coarse movement of the surface to an altitude (distance between nozzle and target surface) of  $0.5d_e$ .

Electrical outputs from the gages were recorded on oscillographs for subsequent data reduction. The response of the instrumentation appeared adequate to measure the desired quantities; however, in some instances, increased accuracy would have been attained by using lower range gages, particularly on the LM model base. Gage response was heavily dependent on the short lengths of plastic tubing which were used to connect orifices on the target surface or LM model base to pressure gages. A time of 0.1 second was chosen as the minimum test-rocket firing time required for all the gages to achieve steady-state response. Overall accuracy of the impingement pressure measurements of the present study is estimated to be  $\pm 10$  percent.

### TEST PROCEDURE

For each test of this investigation the vacuum sphere was initially evacuated to approximately  $4 \times 10^{-4}$  torr. The test rocket was then fired onto one of the solid target surfaces for 0.1 second. (The test rocket achieved steady-state operation within about 60 msec.) The short firing time was desirable to maintain a good simulation of the lunar environment. For the solid-surface impingement tests, the ratio of rocket combustion

pressure to sphere ambient pressure was approximately  $2.8 \times 10^6$  or greater at the time of rocket-thrust termination. The exhaust gas was subsequently evacuated from the vacuum chamber prior to the next test.

Rocket firing time for the particulate-surface impingement tests was increased to 0.5 second to allow sufficient time for a sizable crater to form. For these tests, the ratio of rocket combustion pressure to sphere ambient pressure was only  $6 \times 10^4$  at the time of rocket-thrust termination. The tests were conducted for a constant rocket altitude, and no attempt was made to simulate a realistic descent velocity since the LM model descent-stage retrorocket could not operate at the relatively low combustion-chamber pressure of the LM retrorocket at landing. The vacuum chamber was repressurized and entered after each test to obtain measurements of the surface disturbance and to prepare another surface for the next test.

## RESULTS AND DISCUSSION

The nominal test conditions for impingement of the LM model retrorocket exhaust onto flat and dished target surfaces are listed in table I. Surface impingement pressures, LM model base pressures, and nozzle static pressures were measured during these tests. Several additional tests not listed in table I were conducted on a flat plate to aid in defining the onset of nozzle choking and to measure impingement heating rates. In addition, a few tests were conducted on particulate surfaces to determine the effects of cratering on the LM model base pressures. The results of the experimental study are presented in figures 7 to 18. The surface impingement pressures and the base pressures have been nondimensionalized by dividing them by the rocket combustion pressure. Linear measurements have been nondimensionalized by using the nozzle-exit diameter.

### Surface Impingement Pressures and Heating Rates

Flat surface. - Figure 7(a) presents impingement pressure distributions measured for various rocket altitudes on a flat target surface located normal to the rocket exhaust. Each pressure distribution was obtained by averaging the data from all the pressure orifices located at the same radial location (fig. 3) for at least three tests at different rocket combustion pressures. The pressure distribution changes significantly with rocket altitude. At the highest test altitude ( $h = 3d_e$ ), the pressures are symmetrically distributed across the surface with the maximum pressures occurring at the rocket axis. Lowering the rocket to an altitude of  $2d_e$  increases the rocket-axis impingement pressure but does not otherwise alter the distribution. Further reductions in rocket altitude cause the pressures to distribute in an annular pattern with the maximum pressure occurring away from the rocket axis. Reference 1 attributes this type of pressure

distribution to shock-structure disturbances within the rocket nozzle which produce lower exhaust energy along the rocket axis.

Figure 7(b) presents the results of several normal impingement tests on a flat surface to measure impingement heating rates. The rocket combustion pressure for these tests was  $650 \text{ kN/m}^2$ . Each calorimeter was mounted flush with the surface and was insulated from the surface. The surface heating rates determined by these gages are average values because of the relatively large area of the copper disks. The data indicate that surface heating increases with decreasing rocket altitude and that, in general, the maximum surface heating does not occur at the rocket axis but at a radial location of about  $0.5d_e$  (directly beneath the rocket nozzle lip). The annular distribution of surface heating is similar to the distribution of surface impingement pressures at low rocket altitudes; however, the ratio of maximum heating rate to the rocket-axis heating rate is greater than the similar ratio for surface pressure.

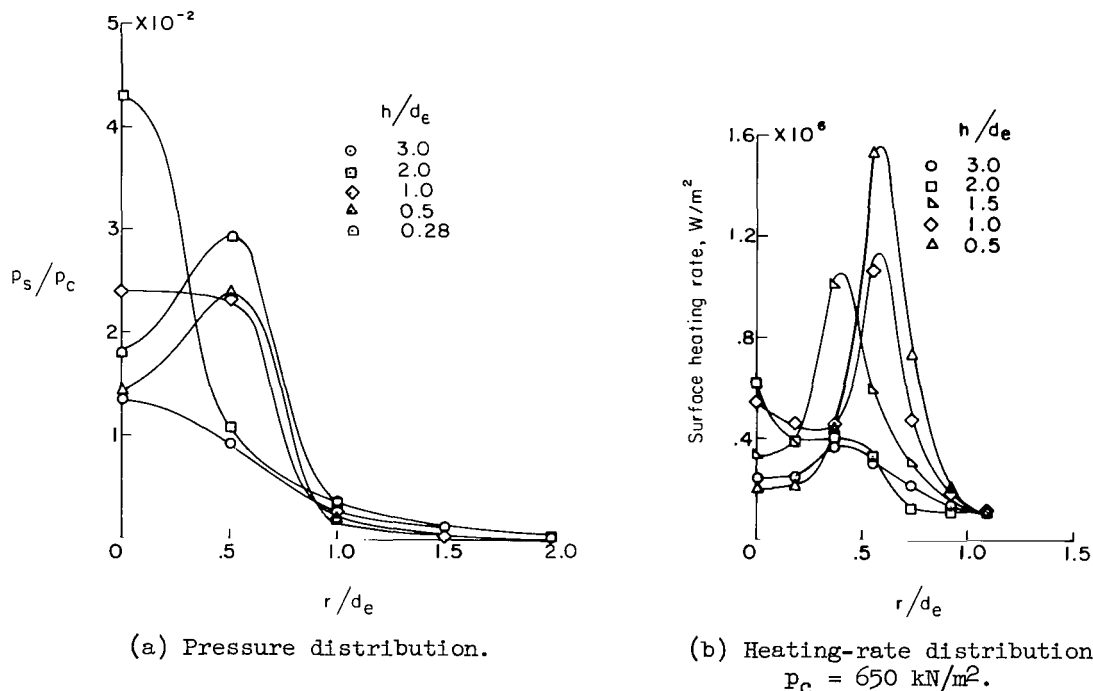
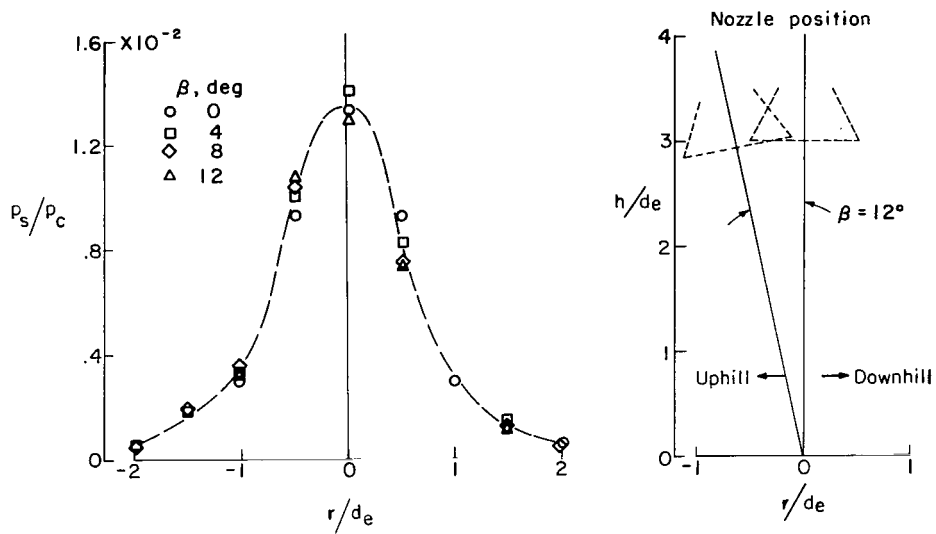
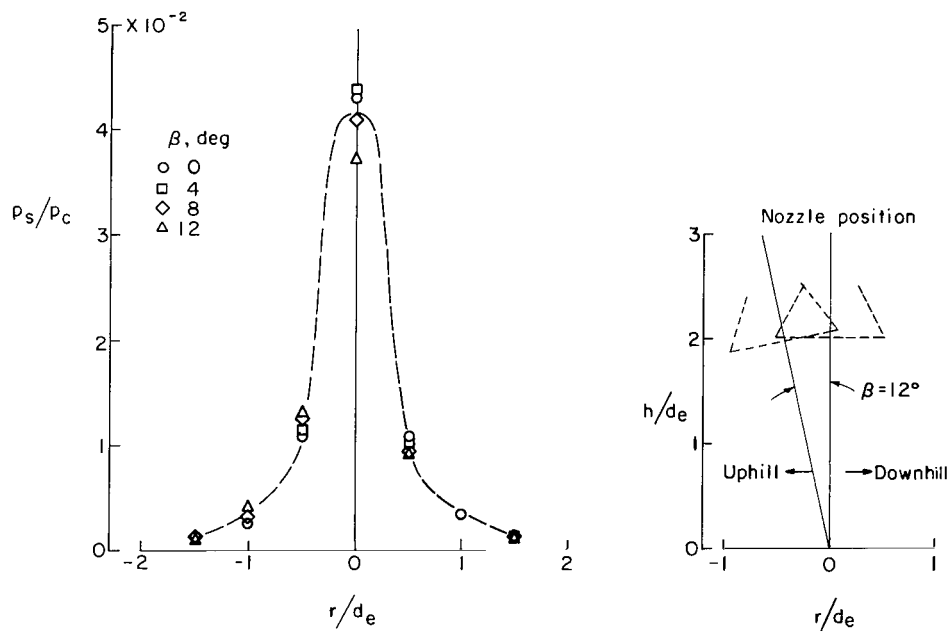


Figure 7.- Effect of rocket altitude on flat-surface pressure and heating-rate distribution.  $\beta = 0^\circ$ .

Figure 8 presents impingement pressure distributions measured for various inclinations of the rocket axis to a flat surface. Each distribution was obtained by averaging the data from pressure orifices 1 to 5 and 21 to 26 (fig. 3) for at least three tests at different rocket combustion pressures. The effect of off-normal rocket-exhaust impingement onto a flat surface is more pronounced at low rocket altitudes. The impingement pressure is higher on the uphill side of the inclined surface and generally appears to increase with increasing surface tilt.

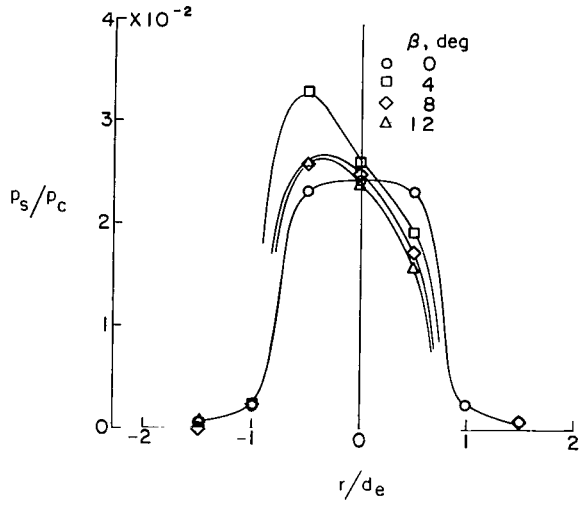


(a)  $h/d_e = 3$ .

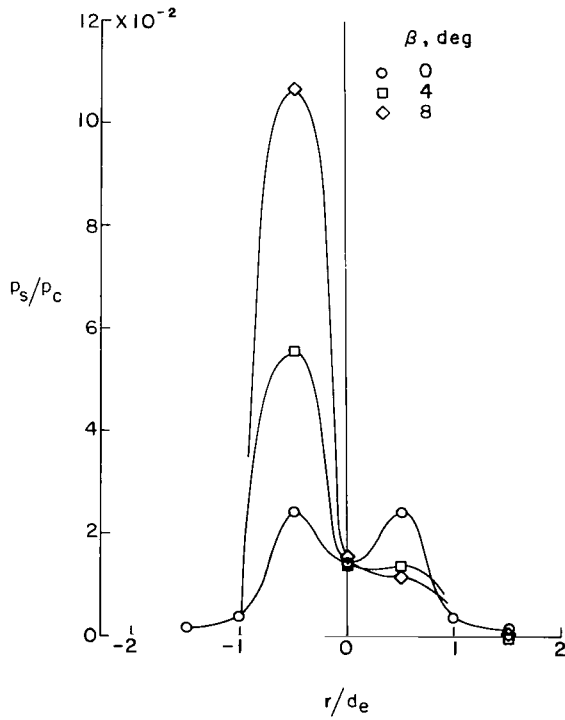


(b)  $h/d_e = 2$ .

Figure 8.- Effect of rocket-axis inclination on flat-surface pressure distribution.

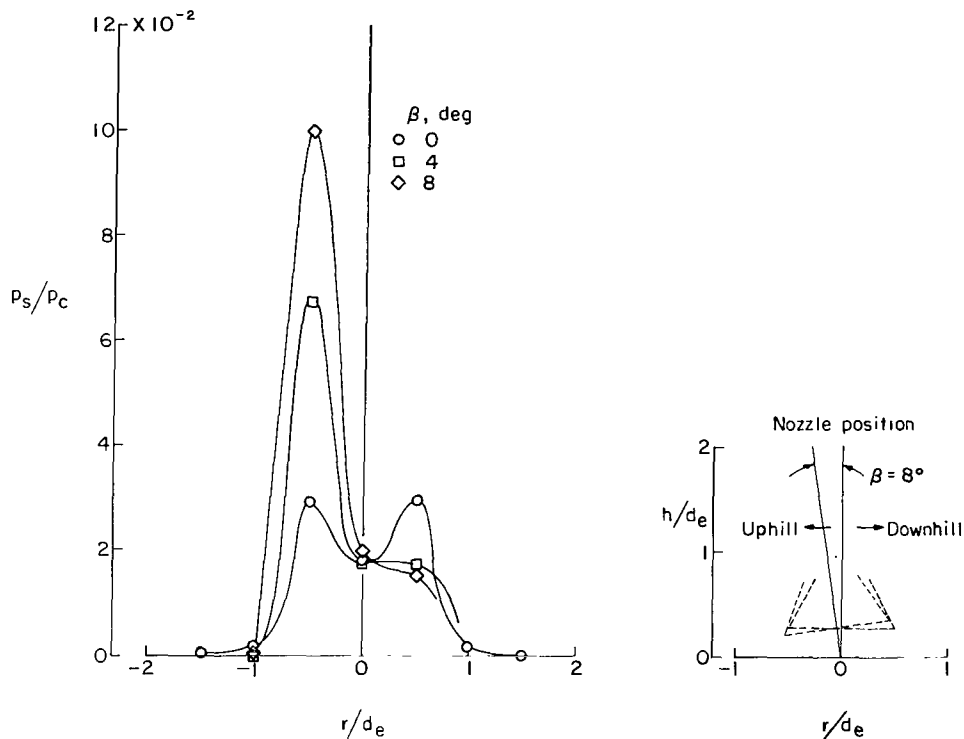


(c)  $h/d_e = 1.0$ .



(d)  $h/d_e = 0.5$ .

Figure 8.- Continued.



(e)  $h/d_e = 0.28$ .

Figure 8.- Concluded.

Figure 9 presents the complete flat-surface impingement pressure distribution measured for several tests at  $h/d_e = 0.5$  for a surface inclination of  $8^\circ$ . This figure illustrates the progressive change in pressure from the uphill to the downhill part of the surface. These data were obtained by averaging the results from six tests (two tests at each of three different rocket combustion pressures). As previously noted, the pressure on the uphill part of the surface is higher than that on the downhill part of the surface.

Dished surface.- Figure 10 presents impingement pressure distributions measured for various rocket altitudes on a dished target surface located normal to the rocket exhaust. Each pressure distribution was obtained by averaging the data from all the pressure orifices located at the same radial location (fig. 4) for at least two tests at different rocket combustion pressures. For the dished surface, the pressure distribution depends on the rocket altitude as it does for the flat surface. The impingement pressure distribution changes from a bell shape to an annular shape with decreasing rocket altitude.

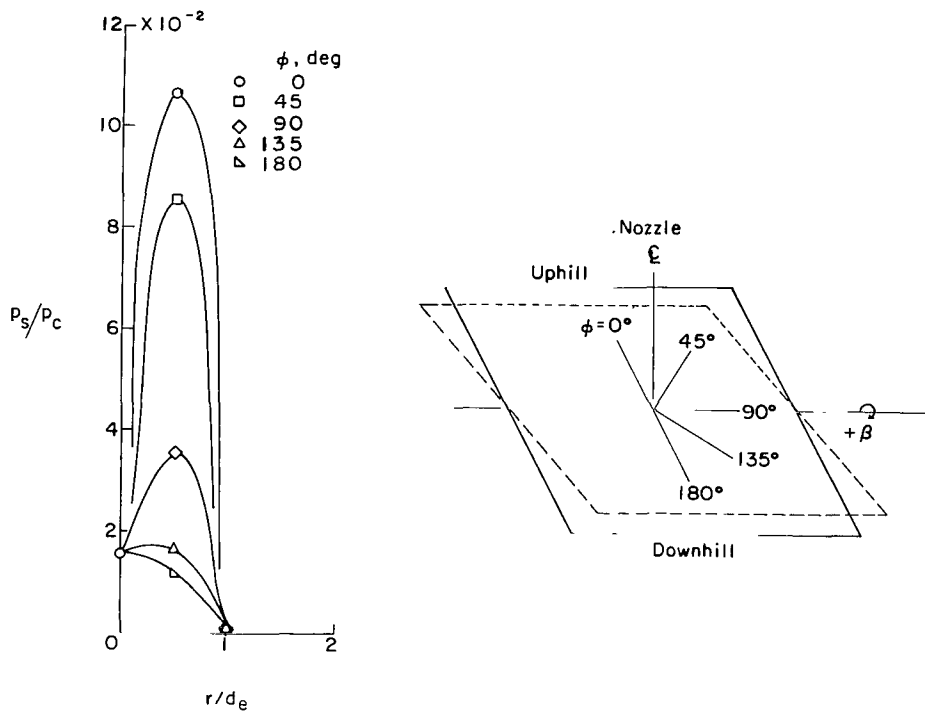


Figure 9.- Complete flat-surface pressure distribution.  
 $\beta = 8^\circ$ ;  $h/d_e = 0.5$ .

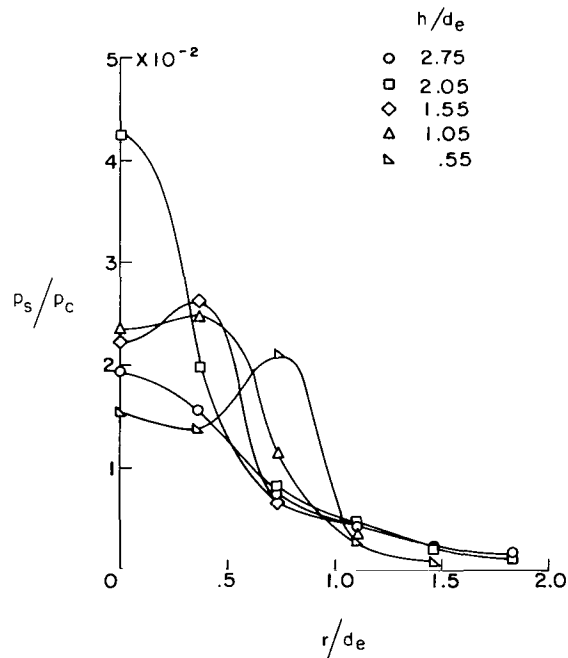
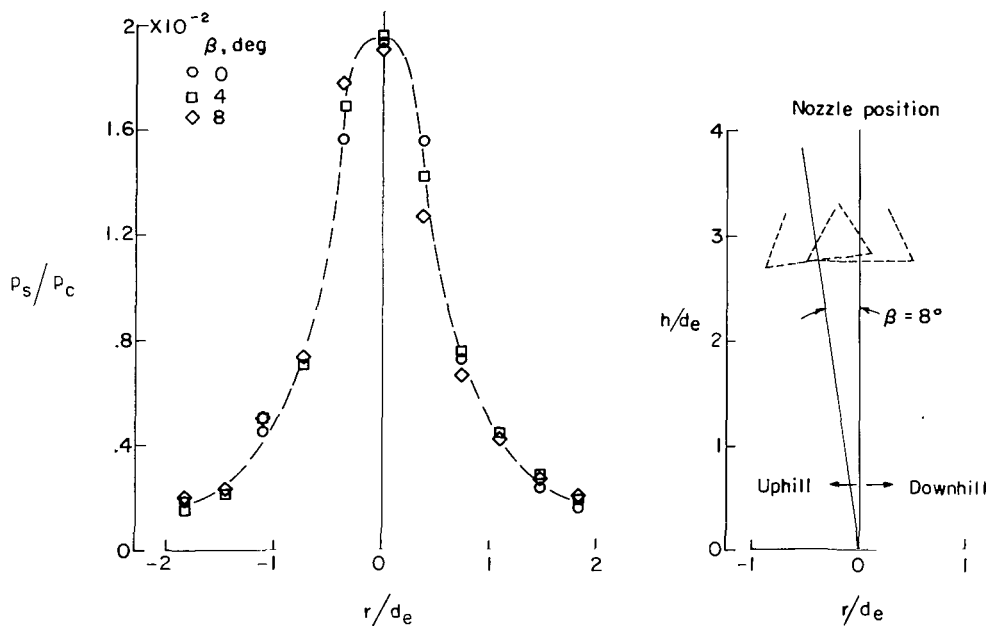


Figure 10.- Effect of rocket altitude  
on dished-surface pressure distribution.  
 $\beta = 0^\circ$ .

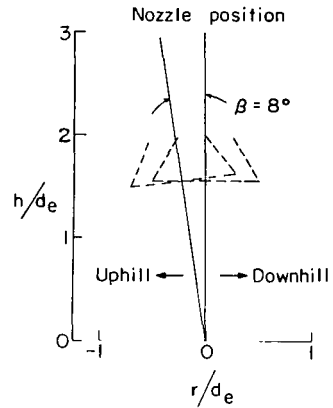
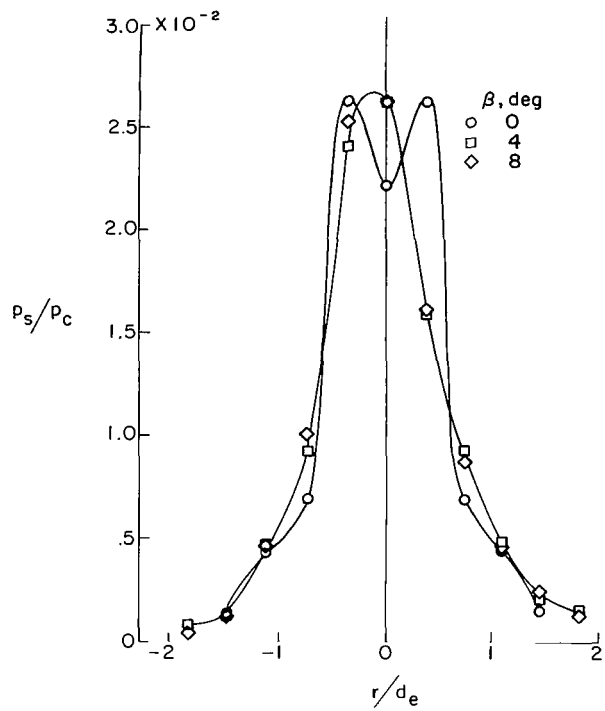
Figure 11 presents impingement pressure distributions measured for various inclinations of the rocket axis to a dished surface. Each distribution was obtained by averaging the data from pressure orifices 1 to 5 and 21 to 26 (fig. 4) for at least three tests at different rocket combustion pressures. At high rocket altitudes, the effect of off-normal rocket-exhaust impingement onto a dished surface is similar to the previously discussed effect for the flat-surface tests. The pressure on the uphill surface area is higher than that on the downhill surface area. However, at the lowest test altitude ( $h = 0.55d_e$ ), inclining the rocket axis to the surface primarily alters the pressure distribution from an annular shape to a bell shape.

Figure 12 presents a summary plot of the variation of rocket-axis impingement stagnation pressure with rocket altitude for all normal impingement tests conducted on flat or dished surfaces. The data show that on both surfaces the rocket-axis pressure increases as the rocket altitude decreases to an altitude of  $2d_e$  and subsequently decreases for a further reduction of altitude. As previously noted, this reduction of the rocket-axis impingement pressure is a result of the changing distribution of surface pressures. The direct dependence of impingement pressure on rocket combustion pressure is represented by the difference in the data for tests at the same rocket altitude but different rocket combustion pressures. The figure shows no discernible effect of surface shape on rocket-axis impingement pressure and therefore is in agreement with the results of reference 9. Two additional data points are included which were obtained during preliminary

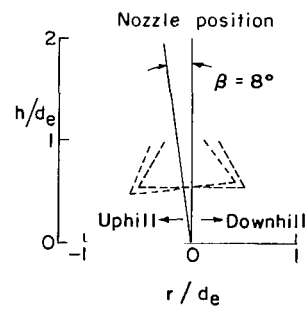
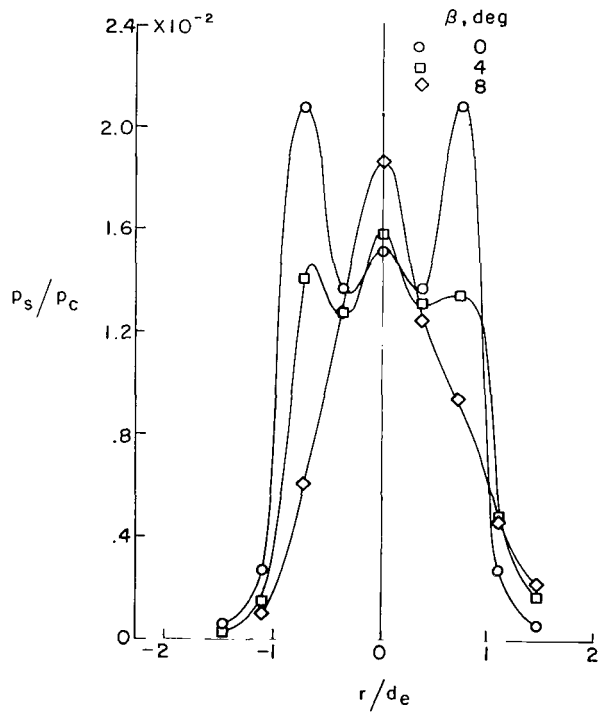


(a)  $h/d_e = 2.75$ .

Figure 11.- Effect of rocket-axis inclination on dished-surface pressure distribution.



(b)  $h/d_e = 1.55$ .



(c)  $h/d_e = 0.55$ .

Figure 11.- Concluded.

tests with the rocket at higher altitudes. The ambient pressure level for these additional tests ( $10^{-2}$  torr) was, however, not as low as for most of the tests presently being reported. Also shown in the figure is the value of normal shock-recovery pressure (based on estimated rocket-exit conditions for one-dimensional frozen flow) which the analysis of reference 3 gives as a limiting surface pressure (about  $4 \times 10^{-2}$ ) at rocket altitudes less than or equal to  $1.14d_e$ . This shock-recovery pressure was only equaled on the target surfaces during the normal impingement tests but was considerably exceeded during off-normal impingement tests on the flat plate, as shown typically by the  $\beta = 8^\circ$  data included in figure 12. These larger surface pressures were measured at  $0.5d_e$  on the uphill side (orifice 25) rather than at the rocket axis (orifice 26) where the surface pressure was substantially less.

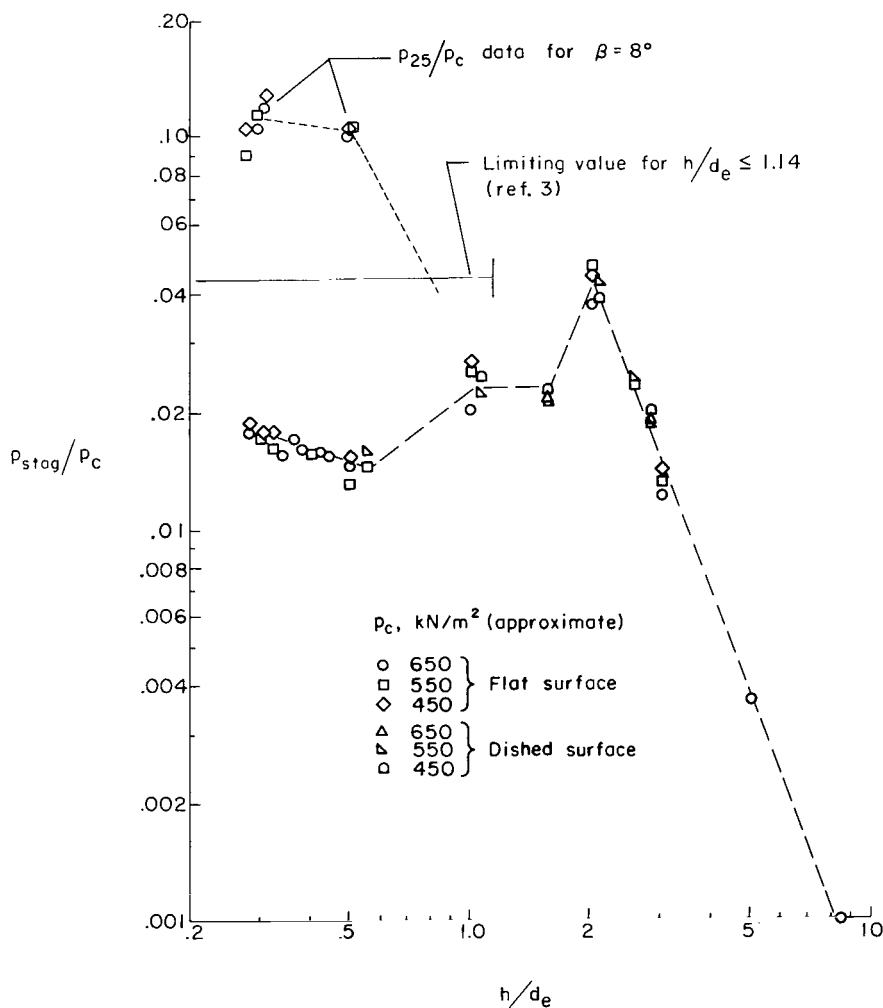


Figure 12.- Effect of rocket altitude on impingement stagnation pressure.  $\beta = 0^\circ$ .

### LM Model Base Pressures

Flat surface. - Figure 13 presents LM model base pressure distributions measured for various rocket altitudes during impingement tests on a flat surface located normal to the rocket exhaust. The distributions shown for  $h/d_e = 0.5$  and  $0.32$  were obtained by averaging the data obtained from three tests at different rocket combustion pressures. The data shown for the lowest rocket altitude, where nozzle choking occurred for an isolated test, may or may not be repeatable. With the test instrumentation used in this investigation, LM model base pressures were initially detectable at an altitude of  $0.75d_e$ . The figure shows that LM model base pressures increase with decreasing rocket altitude and that, except for the test in which nozzle choking occurred, these pressures were symmetrically distributed on the LM base.

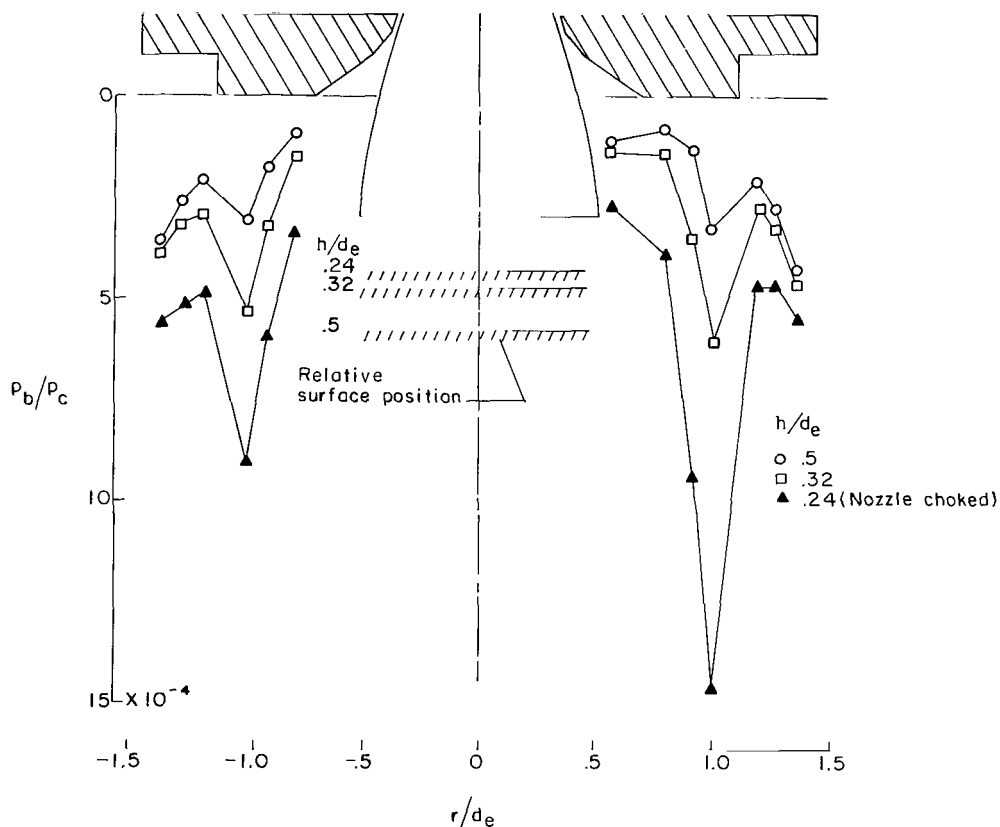
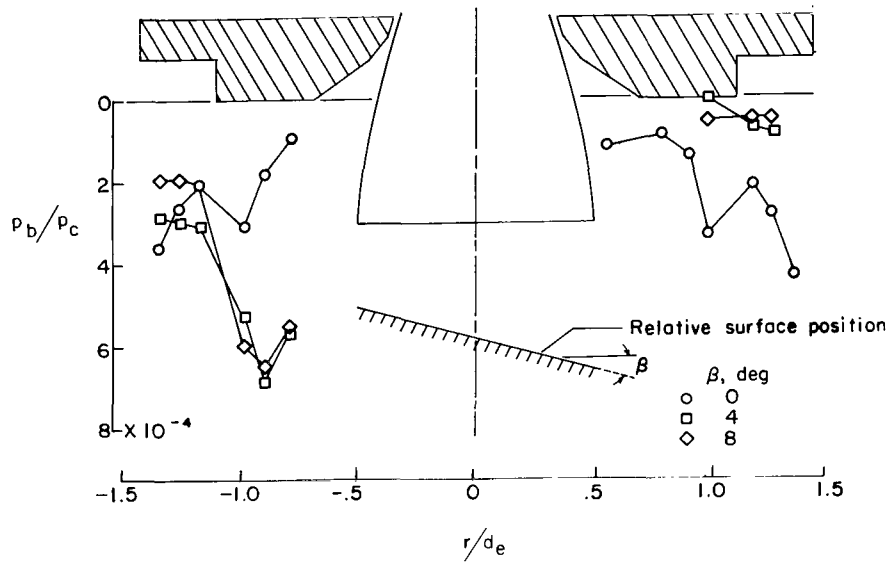


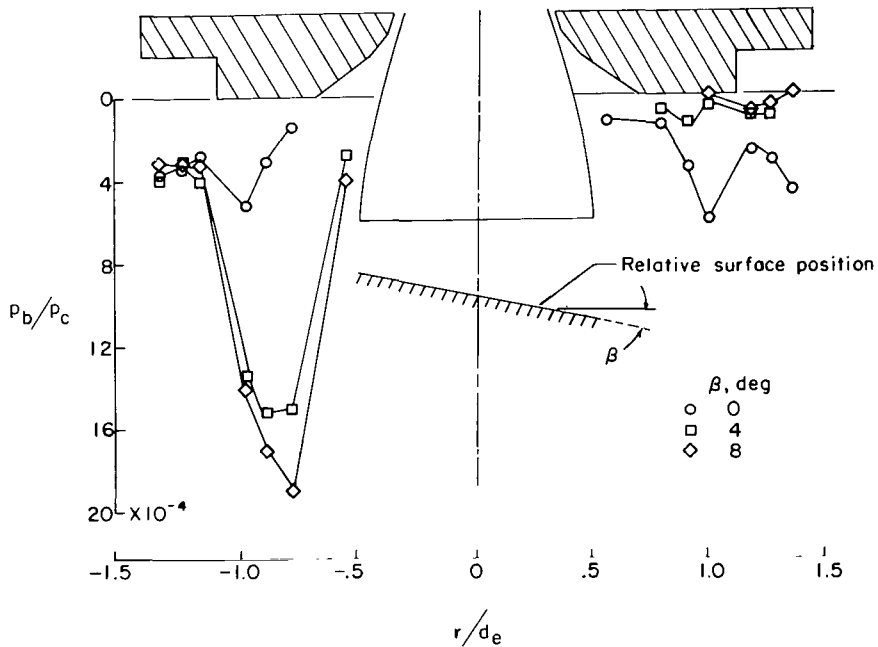
Figure 13.- Effect of rocket altitude on LM model base pressures for flat-surface impingement.  $\beta = 0^\circ$ .

Figure 14 presents LM model base pressure distributions measured for various inclinations of the rocket axis to a flat surface. Each distribution was obtained by averaging the data for three tests at different rocket combustion pressures. Since the LM model base was instrumented along two perpendicular rays (fig. 2(a)), it was necessary to repeat

the tests with the LM model base rotated  $180^\circ$  in order to obtain the pressure distributions shown. The data show that pressures for off-normal impingement increase on the part of the LM base which is closest to the surface and decrease on the part which is farthest from the surface. These pressures would tend to stabilize the LM vehicle by inducing a moment which would act to align the rocket exhaust normal to the impingement surface.



(a)  $h/d_e = 0.5$ .



(b)  $h/d_e = 0.32$ .

Figure 14.- Effect of rocket-axis inclination on LM model base pressures for flat-surface impingement.

Dished surface.- Figure 15 presents LM model base pressure distributions measured for various inclinations of the rocket axis to a dished surface at a rocket altitude of  $0.55d_e$ . LM model base pressures were initially detectable at an altitude of  $1.05d_e$ . The fact that repeat tests were not conducted on the curved surface with the LM model base rotated  $180^\circ$  accounts for the incomplete pressure distributions shown. The limited data presented are the average pressures measured from three tests at different rocket combustion pressures. The data indicate decreasing base pressures on the part of the base which moves away from the surface. This result is similar to that of the previously discussed flat-surface tests. The LM model base pressures shown are higher than those for a comparable test on a flat surface (fig. 14(a)); therefore, the curved impingement surface apparently focuses more of the exhaust back toward the model spacecraft.

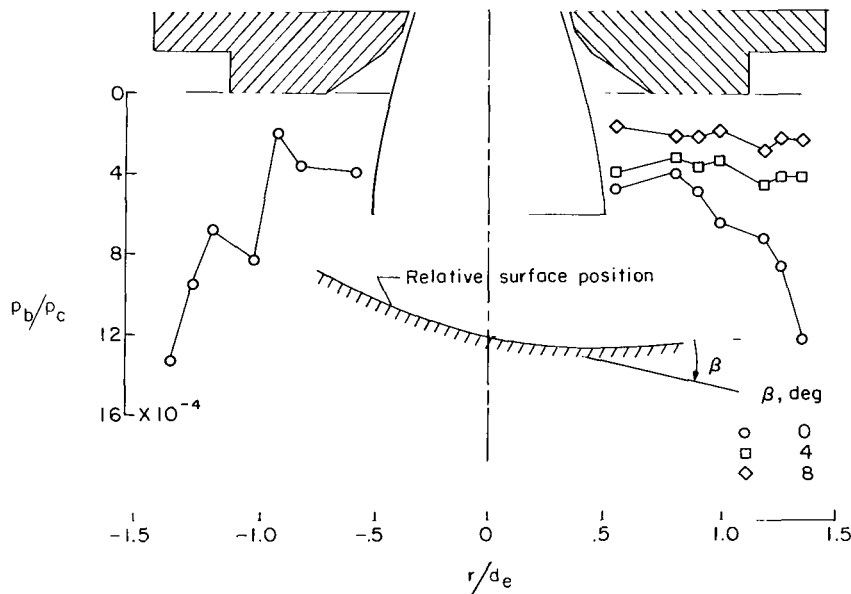
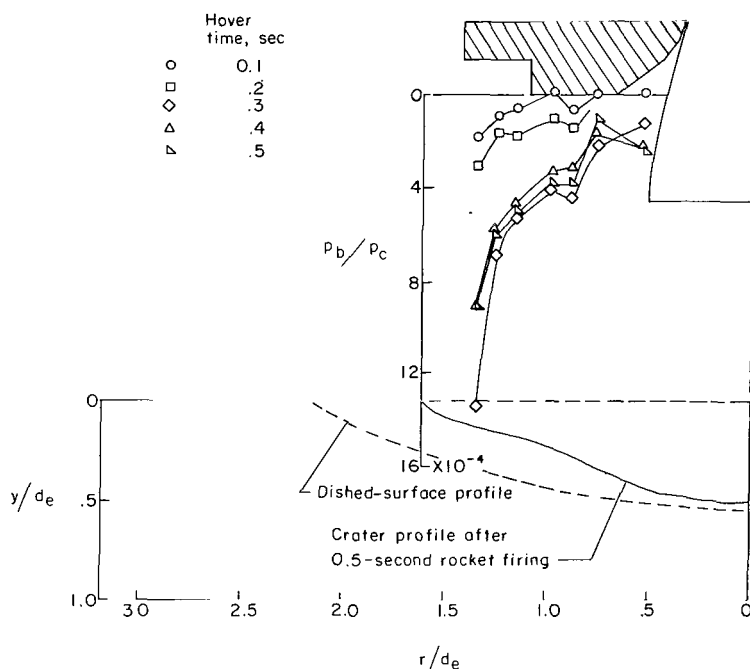


Figure 15.- Effect of rocket-axis inclination on LM model base pressures for dished-surface impingement.  $h/d_e = 0.55$ .

Particulate surface.- Figure 16 presents typical results obtained during impingement tests on noncohesive particulate surfaces, which are easily disturbed by impinging rocket-exhaust gases. The LM model base pressures shown are the average pressures measured by gages located at the same radial station (fig. 2(a)) for various times during the 0.5-second duration of rocket firing. Data are presented for two different noncohesive particulate surfaces at similar rocket conditions. During both tests, significant base pressures were measured for different amounts of surface disturbance. The crater profiles shown in figure 16 are the average radial profiles measured after repressurization

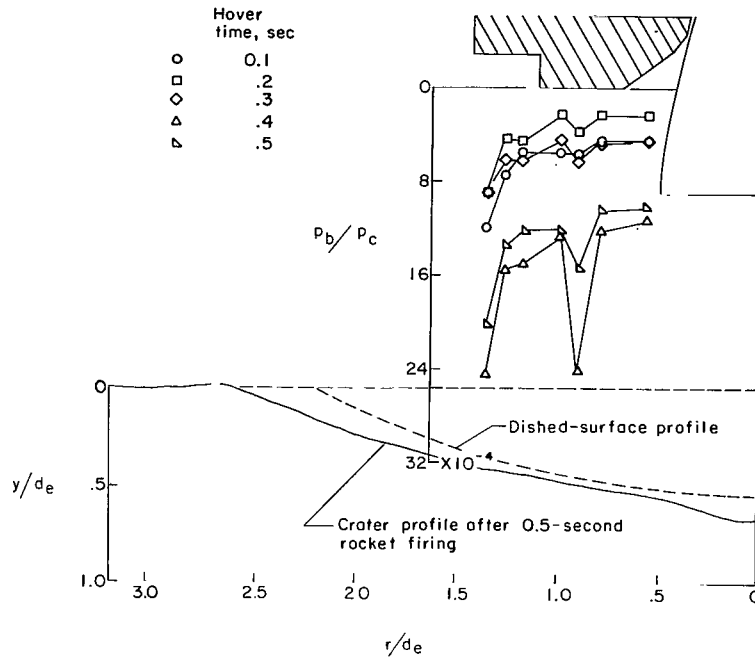
and entry into the vacuum sphere. The base pressures changed during the test as the surface contour was altered by the impinging exhaust gases. At the test rocket altitude of  $1d_e$ , LM model base pressures were not detected during flat-surface tests, but they were detected during dished-surface tests. The LM model base pressures measured during the particulate-surface tests were, however, considerably larger than those detected during dished-surface tests although the final crater profiles were not greatly different from that of the dished surface. Additional tests (not presented) were conducted on particulate surfaces at a rocket altitude of  $2.2d_e$ . Although the craters were comparable in size with those measured at the lower rocket altitude, no LM model base pressures were detected.

In summary, figure 17 presents the variation of the maximum base pressure with rocket altitude for tests on flat, dished, and particulate surfaces. Included are data measured during both normal and off-normal impingement tests at different rocket combustion pressures. The data presented for the particulate-surface tests are positioned at the approximate value of  $h/d_e$  at the time of the pressure measurement, determined by assuming that the crater depth increased linearly with time. The data values presented for the dished-surface tests would be higher if tests had been conducted with the LM model base pressure orifices aligned with the surface at its closest approach. The figure



(a) Mixture;  $p_c = 434 \text{ kN/m}^2$ .

Figure 16.- Effect of rocket-exhaust impingement on particulate surfaces.  $\beta = 0^\circ$ ;  $h/d_e = 1$ .



(b) Sand;  $p_c = 455 \text{ kN/m}^2$ .

Figure 16.- Concluded.

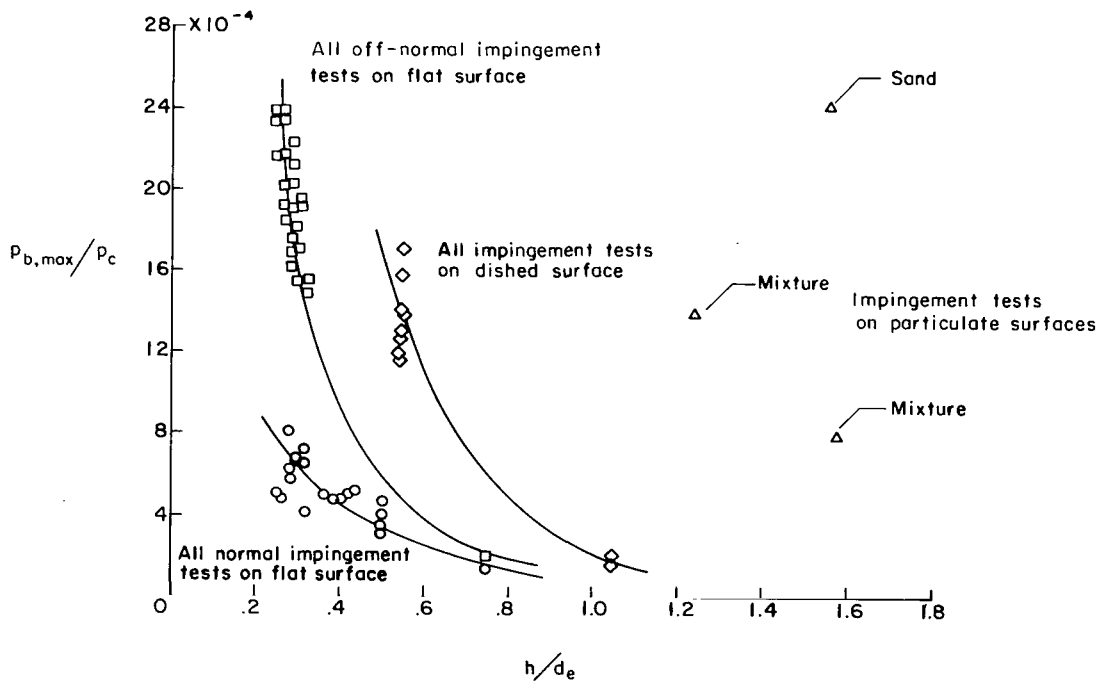


Figure 17.- Effect of rocket altitude on LM model maximum base pressure.

shows that surface contour determines the amount of rocket-exhaust gases which are redirected toward the model spacecraft. Over the range of test parameters investigated, the LM model base pressures measured were one to two orders of magnitude lower than the target-surface impingement pressures.

### Nozzle Choking

During some of the flat-surface tests, the LM model retrorocket was caused to choke by reducing the rocket altitude below a critical value. Measured nozzle static-pressure distributions which indicate a choked-flow condition are summarized in figure 18 as a function of nozzle-area ratio. Multiple data points at a given nozzle station are from repeat tests at different rocket combustion pressures. The effect of nozzle choking is a significant increase in nozzle static pressures compared with unchoked values. The onset of nozzle choking depends upon both rocket attitude and altitude. The dependence on rocket attitude may reflect some nonuniformity of the exhaust gases issuing from the test rocket. The critical rocket altitude for choking seems to be approximately the altitude at which the cylindrical escape area, formed between the rocket exit and the surface, becomes less than the rocket-exit area (which occurs for a rocket altitude of  $0.25d_e$ , independent of  $\beta$ ).

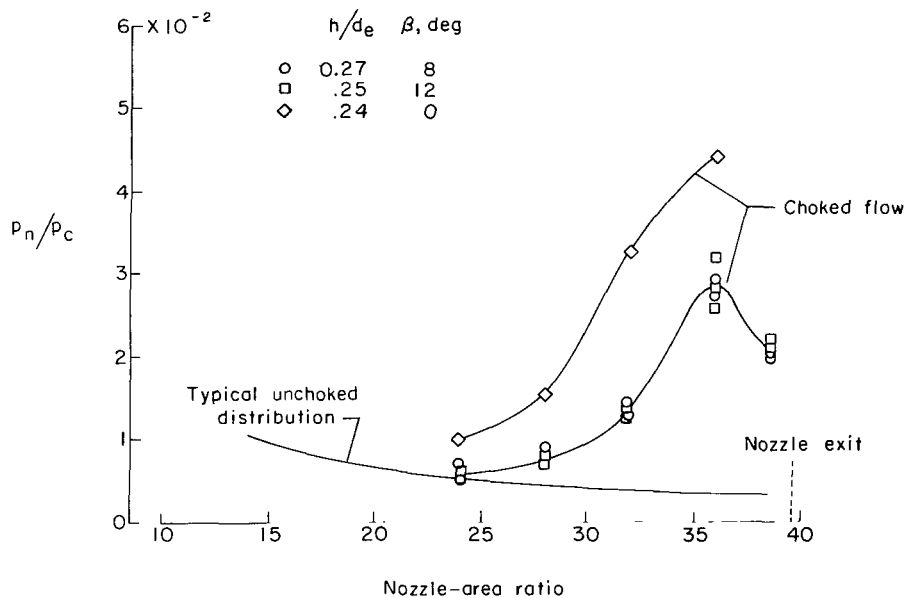


Figure 18.- Effect of flat-surface proximity on test-rocket nozzle static pressures.

## CONCLUDING REMARKS

An experimental program was conducted to investigate the effects of rocket-exhaust impingement on close-range surfaces. The configuration used in this investigation simulated the Apollo lunar module during lunar landing. The following remarks are considered to be generally applicable to similar programs.

Normal impingement pressures are inversely proportional to rocket altitude but approach limiting maximum values at an altitude of approximately two rocket-exit diameters. For normal impingement onto flat or dished surfaces, the surface pressure distribution changes from a bell shape to an annular shape below a rocket altitude of about 2 rocket-exit diameters. Also, the maximum surface pressure equaled the value of shock-recovery pressure (based on estimated rocket-exit conditions for one-dimensional frozen flow). This pressure was, however, considerably exceeded during off-normal tests on a flat surface at low rocket altitudes.

Surface heating rates measured for normal impingement onto a flat surface indicate that surface heating increases with decreasing rocket altitude and that, in general, the maximum surface heating does not occur at the rocket axis but rather at a radial location of about 0.5 rocket-exit diameter (directly beneath the rocket nozzle lip).

Pressures on the base of the model spacecraft were not measurable during impingement tests on flat and dished solid surfaces until the model descended to a rocket altitude of 0.75 and 1.05 rocket-exit diameters, respectively. During impingement and erosion of noncohesive particulate surfaces, however, base pressures were measurable at an altitude of 1 rocket-exit diameter. The pressures on the base of the model spacecraft caused by surface-reflected exhaust gases were one to two orders of magnitude lower than the target-surface impingement pressures. The distribution of these base pressures depends upon the attitude of the rocket with respect to the impingement surface. The magnitude of these base pressures was dependent upon the contour of the target surface as evidenced by the relatively high pressures recorded during impingement and erosion of particulate target surfaces.

The onset of nozzle choking as a result of surface proximity occurred at approximately the altitude at which the cylindrical escape area, formed between the rocket exit and the target surface, became less than the rocket-exit area (a rocket altitude of 0.25 rocket-exit diameter).

Langley Research Center,  
National Aeronautics and Space Administration,  
Hampton, Va., May 4, 1970.

## REFERENCES

1. Stitt, Leonard E.: Interaction of Highly Underexpanded Jets With Simulated Lunar Surfaces. NASA TN D-1095, 1961.
2. Stitt, Leonard E.; and Latto, William T., Jr.: Highly Underexpanded Exhaust Jets Against Adjacent Surfaces. Astronaut. Aerosp. Eng., vol. 1, no. 1, Feb. 1963, pp. 107-110.
3. Roberts, Leonard: The Action of a Hypersonic Jet on a Dust Layer. Pap. No. 63-50, Inst. Aerosp. Sci., Jan. 1963.
4. Roberts, Leonard; and South, Jerry C., Jr.: Comments on Exhaust Flow Field and Surface Impingement. AIAA J. (Technical Comments), vol. 2, no. 5, May 1964, pp. 971-974.
5. Land, Norman S.; and Clark, Leonard V.: Experimental Investigation of Jet Impingement on Surfaces of Fine Particles in a Vacuum Environment. NASA TN D-2633, 1965.
6. Vick, Allen R.; and Andrews, Earl H., Jr.: An Investigation of Highly Underexpanded Exhaust Plumes Impinging Upon a Perpendicular Flat Surface. NASA TN D-3269, 1966.
7. Christensen, E. M.; Batterson, S. A.; et al.: Lunar Surface Mechanical Properties. Surveyor V Mission Report - Part II: Science Results, Tech. Rep. 32-1246 (Contract No. NAS 7-100), Jet Propulsion Lab., California Inst. Technol., Nov. 1, 1967, pp. 43-88.
8. Land, Norman S.; and Scholl, Harland F.: Scaled Lunar Module Jet Erosion Experiments. NASA TN D-5051, 1969.
9. Clark, Leonard V.: Free Jet Impingement Normal to a Curved Surface in a Vacuum. NASA TN D-3920, 1967.

TABLE I. - NOMINAL TEST CONDITIONS FOR ROCKET-EXHAUST  
IMPINGEMENT ONTO SOLID SURFACES

Rocket altitude Exit diameter, $h/d_e$	Rocket combustion pressure, $kN/m^2$	Surface or rocket-axis inclination, $\beta$ , deg
	Flat surface	
3	650, 550, 450	0, 4, 8, 12
2	650, 550, 450	0, 4, 8, 12
1	650, 550, 450	0, 4, 8, 12
.5	650, 550, 450	0, 4, 8, 12
.44	650	0
.42	650	0
.40	650	0
.38	650	0
.36	650	0
.34	650	0
.32	650, 550, 450	0, 4, 8, 12
.30	650, 550, 450	0, 4, 8, 12
.28	650, 550, 450	0, 4, 8, 12
	Dished surface	
2.75	650, 550, 450	0, 4, 8
2.55	550, 450	0
2.05	550, 450	0
1.55	650, 550, 450	0, 4, 8
1.05	550, 450	0
.55	650, 550, 450	0, 4, 8